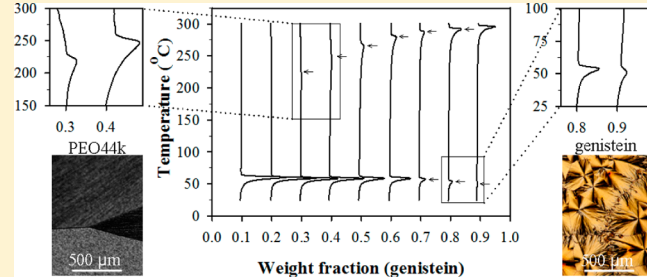


# Solubilization of Genistein in Poly(oxyethylene) through Eutectic Crystal Melting

Sasiwimon Buddhiranon and Thein Kyu\*

Department of Polymer Engineering, University of Akron, Akron, Ohio 44325-0301, United States

**ABSTRACT:** Solid–liquid phase diagrams of binary crystalline blends of genistein with poly(ethylene oxide) (PEO) and poly(ethylene glycol) (PEG) were established experimentally and theoretically based on the combined Flory–Huggins free energy of liquid–liquid phase separation and the phase field free energy pertaining to crystal solidification. The liquidus lines obtained self-consistently were found to agree well with trends of depressed crystal melting transitions in genistein/PEO and genistein/PEG blends, exhibiting eutectic phase behavior. Of particular importance is the lowering of the eutectic temperature of the genistein/PEO blend by about 60 °C upon switching to the genistein/PEG system. The occurrence of interspecies hydrogen bonding between genistein molecules and both PEO and PEG chains, albeit weak, was noticed by Fourier transform infrared spectroscopy. The improved solubility of genistein in PEG can be attributed not only to lowering of the molecular weight of PEG utilized, but also to its terminal hydroxyl groups. This eutectic melting approach by PEG solvent is sufficiently effective in solubilizing genistein crystals that development of genistein-containing drugs might be feasible for injection and/or oral administration.



## INTRODUCTION

Phytoestrogens are weak hormones found in many plants such as whole grains, beans, leafy greens, fruits, and seed oils. These phytochemicals exhibit various biological/pharmacological activities. One phytoestrogen that belongs to the isoflavone class is genistein (5,7,4'-trihydroxyisoflavone), which is especially attractive because of its tyrosine kinase inhibitory, anticarcinogenic, antioxidant, anti-inflammatory, and antimicrobial activities.<sup>1,2</sup> Additionally, genistein has been shown to inhibit skin damage induced by UV irradiation<sup>3</sup> and to stimulate human fibroblast collagen synthesis.<sup>4</sup> Thus, research for potential uses of genistein in oral and topical applications has been of immense interest. Genistein falls into class II of the biopharmaceutical classification system (BCS) by virtue of its low solubility (only  $3 \times 10^{-6}$  mol·L<sup>-1</sup> in water)<sup>5</sup> and high permeability.<sup>6</sup> Because of the problem of inherently low aqueous solubility and low dissolution rate, over 70% of all potentially active drugs have failed to reach the market.<sup>7</sup> To overcome these hurdles, it is essential to find appropriate solvents for hydrophobic drugs such as genistein.

A common practice in solubilizing water-insoluble compounds is the addition of water-soluble cosolvents to the formulation. Water-soluble cosolvents can enhance the solubility of nonpolar solutes by several orders of magnitude. Following the principle of “like dissolves like”,<sup>8</sup> the polarity of water should be reduced by mixing it with other hydrophilic substances, thus increasing the solubility of nonpolar compounds. The use of surface-active agents, micellization, and complexation has been widely applied. However, the resulting prodrug and salt formation requires additional animal studies to confirm their efficacy and toxicity.<sup>7</sup>

Another conventional approach is to take advantage of the melting point depression of crystalline/noncrystalline mixtures to improve the solubility of drug crystals in appropriate solvents.<sup>9</sup> Alternatively, the eutectic crystal melting approach can be employed by codissolving small-molecule drug crystals in crystalline organic compounds or polymeric matrixes. The proposed cosolvation strategy is advantageous not only in dramatically raising drug solubility, but also in its simplicity in formulation. We have identified poly(oxyethylene) (POE) of low molar mass [i.e., poly(ethylene glycol) (PEG)] and its higher-molecular-weight analogue poly(ethylene oxide) (PEO) as potential candidates, both of which are water-soluble, biocompatible, and abundantly available commercially in a variety of molecular weights. The hydrophilic behavior and availability of these two materials contribute to their wide use across several therapeutic treatments and also in food industries. Moreover, PEG has been approved by the U.S. Food and Drug Administration (FDA) for both oral and topical applications. PEG has been used as a carrier in various pharmaceutical formulations, foods, and cosmetics.<sup>10</sup> The present work focuses on eutectic phase diagrams of binary crystalline blends of genistein with PEO and PEG as a means of solubilizing the genistein crystals and evaluating potential use of PEO and/or PEG as a water-soluble carrier molecule for genistein.

Received: March 20, 2012

Revised: June 12, 2012

Published: June 15, 2012

## ■ EXPERIMENTAL AND THEORETICAL METHODS

**Materials and Sample Preparation.** Poly(ethylene oxide) (PEO) was purchased from Sigma-Aldrich. The number-average molecular weight ( $\bar{M}_n$ ) and weight-average molecular weight ( $\bar{M}_w$ ) of PEO were determined by means of high-permeation liquid chromatography (HPLC) using polystyrene standards. The  $\bar{M}_n$  and  $\bar{M}_w$  values should be regarded as estimates and were found to be  $4.44 \times 10^4$  and  $5.02 \times 10^4$  g/mol, respectively. Two poly(ethylene glycol) samples with different molecular weights, namely,  $\bar{M}_n = 6.70 \times 10^3$  and  $4.60 \times 10^2$  g/mol, were purchased from Sigma-Aldrich and Polymer Source, Inc.; they are hereafter designated as PEG7k and PEG460, respectively. The estimated  $\bar{M}_n$  value and molecular weight distribution ( $\bar{M}_w/\bar{M}_n$ ) of each sample are listed in Table 1, along with other physical characteristics of the polymers.

**Table 1.**  $\bar{M}_n$ ,  $\bar{M}_w/\bar{M}_n$ ,  $T_g$ , and  $T_m$  Values and Identification Codes of the Samples<sup>a</sup>

sample	$\bar{M}_n$ (g·mol <sup>-1</sup> )	$\bar{M}_w/\bar{M}_n$	$T_g$ (°C)	$T_m$ (°C)	code
poly(ethylene oxide)	$4.44 \times 10^4$	1.13	-48	65	PEO44k
poly(ethylene glycol)	$6.70 \times 10^3$	1.04	-	57	PEG7k
poly(ethylene glycol)	$4.60 \times 10^2$	1.10	-	2	PEG460

<sup>a</sup> $\bar{M}_n$  and  $\bar{M}_w$  were estimated by HPLC (model 1515 instrument, Waters) with polystyrene standards.

Genistein ( $C_{15}H_{10}O_5$ , molecular weight 270 g/mol) was obtained from MDidea Exporting Division (YinChuan, China) with >98% purity. Tetrahydrofuran (THF), from Sigma-Aldrich, was used as a common solvent. All materials were used as received without further purification.

Genistein and PEO were dissolved in THF in varying compositions to form 5 wt % THF solutions. Films were cast on glass slides from the THF solutions and evaporated under ambient conditions for 24 h. Subsequently, the films were dried at 50 °C for 2 days under a vacuum to remove residual solvent. The average film thickness was about 10 μm. The physical and morphological properties of the blend samples were characterized by differential scanning calorimetry (DSC), thermogravimetric analysis (TGA), polarized optical microscopy (POM), and Fourier transform infrared (FTIR) spectroscopy.

**Methods.** Thermal stability was examined using a thermogravimetric analyzer (TA Instruments, Q 50). As-received genistein and polymers and their mixtures were subjected to thermogravimetric analysis (TGA) by ramping at a heating rate of 10 °C/min from 25 to 600 °C under nitrogen gas circulation. The flow rate was 50 mL/min. The degradation temperature ( $T_d$ ) was estimated from the point of 5% weight loss in the TGA thermogram.

DSC measurements were performed on solution-cast samples under a nitrogen atmosphere using a TA Instruments Q 200 differential scanning calorimeter. Samples in the recommended amount of approximately 5 mg were encapsulated in hermetic pans and then scanned at a heating rate of 5 °C/min. Indium ( $T_m = 156.6$  °C) standard was used for temperature calibration. In the first DSC scan, the samples were heated to 300 °C to remove thermal prehistory. Only the second heating scan from -90 to 350 °C was used in the analysis. Glass transition temperatures were measured from the

inflection point of the DSC thermograms, and melting points were determined from the endothermic peak positions.

The interaction between genistein and POE was analyzed by means of FTIR spectroscopy. Infrared spectra of all genistein/PEO and genistein/PEG blends were acquired by depositing the samples on standard KBr discs. The FTIR samples were solution-cast on KBr discs from 5 wt % solution in THF and dried under a vacuum at 50 °C for 24 h to ensure complete removal of any residual solvent. Film thickness was adjusted to obey the Beer-Lambert law. Infrared spectra were acquired using a Thermo Scientific Nicolet 389 FTIR spectrophotometer over a range of 400–4000 cm<sup>-1</sup>. The IR spectra were averaged from 32 scans with a resolution of 4 cm<sup>-1</sup>. To avoid the problem of moisture absorption in PEO, all IR scans were collected at 100 °C inside a temperature-controlled chamber.

The development of phase morphology was examined on an optical microscope (BX60, Olympus) using a sample hot stage and a temperature controller (TMS 93, Linkam). For DSC and TGA experiments, all samples were prepared under similar solvent-casting conditions in Petri dishes and stored in desiccators until use. However, in the POM and FTIR studies, thin films were directly cast on cover glass slides and KBr disks, respectively. The microstructures were photographed using a 35-mm digital camera (Canon, EOS 400D) at 50× magnification, following several thermal quenches into various coexistence regions from the isotropic melt.

**Thermodynamic Modeling of Eutectic Phase Diagram.** It is a fundamental principle of thermodynamics that materials always tend to approach a state of minimum free energy until equilibrium is reached. The free energy of liquid–liquid mixing can be described in the framework of Flory–Huggins (FH) theory as<sup>11</sup>

$$f_{\text{mixing}} = \frac{\phi_1 \ln \phi_1}{r_1} + \frac{\phi_2 \ln \phi_2}{r_2} + \chi_{\text{FH}} \phi_1 \phi_2 \quad (1)$$

where  $\phi_1$  and  $\phi_2$  are the volume fractions of components 1 and 2, respectively, that satisfy the incompressibility condition (i.e.,  $\phi_1 + \phi_2 = 1$ ). The parameters  $r_1$  and  $r_2$  represent the numbers of statistical segments of each constituent. The FH interaction parameter ( $\chi_{\text{FH}}$ ), representing the amorphous–amorphous interaction, can be given empirically as  $\chi_{\text{FH}} = \chi_{\text{aa}} = A + B/T$ , where  $A$  and  $B$  are constants.

The anisotropic free energy pertaining to the crystalline order parameter can be described in the context of phase field theory using a Landau-type asymmetric free energy.<sup>12</sup> We extended the phase field theory to binary crystalline polymer blends, in which the local free energy density of the two-component crystalline system is given as<sup>13</sup>

$$\begin{aligned} f_{\text{local}}(\psi_i) &= W_i \int_0^{\psi_i} \psi_i (\psi_i - \zeta_{0,i})(\psi_i - \zeta_i) d\psi_i \\ &= W_i \left[ \zeta_i \zeta_{0,i} \frac{\psi_i^2}{2} - (\zeta_i + \zeta_{0,i}) \frac{\psi_i^3}{3} + \frac{\psi_i^4}{4} \right] \end{aligned} \quad (2)$$

where  $\zeta_{0,i}$  represents the crystalline order parameter at the stable energy well and  $\zeta_i$  corresponds to the crystalline order parameter of the unstable energy barrier for the crystal solidification to overcome.  $W_i$  is a dimensionless coefficient associated with the energy barrier, and  $i = 1$  or  $2$ .

The total free energy density of the genistein/POE system can be expressed as the weighted sum of the free energy densities of crystal solidification of the crystalline constituents

$[f(\psi_1)$  and  $f(\psi_2)]$  with their corresponding volume fractions in conjunction with the coupling anisotropic interaction terms that account for crystalline–amorphous, amorphous–crystalline, and crystalline–crystalline interactions as follows<sup>13</sup>

$$\begin{aligned} f(\psi_1, \psi_2, \phi_1, \phi_2) = & \phi_1 f(\psi_1) + \phi_2 f(\psi_2) + \frac{\phi_1}{r_1} \ln \phi_1 \\ & + \frac{\phi_2}{r_2} \ln \phi_2 + [\chi_{\text{ca}} + (\chi_{\text{ca}} \psi_1^2 - 2\chi_{\text{cc}} \psi_1 \psi_2 + \chi_{\text{ac}} \psi_2^2)] \phi_1 \phi_2 \end{aligned} \quad (3)$$

The first and second terms represent the Landau-type phase field free energy of crystal solidification of each component in which the individual free energy of the constituents is weighted by the respective volume fractions,  $\phi_1$  and  $\phi_2$ . The third and fourth terms represent the entropic contributions to the free energy of mixing of the amorphous constituents. The  $\chi_{\text{FH}} = \chi_{\text{aa}}$  parameter in the fifth term (the first term in the brackets) represents the amorphous–amorphous interaction parameter of Flory–Huggins theory that characterizes the liquid–liquid demixing. The anisotropic interactions such as crystalline solid 1–amorphous liquid 2 or amorphous liquid 1–crystalline solid 2, denoted as  $\chi_{c_1 c_2} \equiv \chi_{\text{ca}}$  and  $\chi_{a_1 c_2} \equiv \chi_{\text{ac}}$ , respectively, can be taken as proportional to the enthalpy of crystal fusion of each constituent ( $\Delta H_1^c$  and  $\Delta H_2^c$ ), that is,  $\chi_{\text{ca}} \propto \Delta H_1^c / RT$  and  $\chi_{\text{ac}} \propto \Delta H_2^c / RT$ . According to Matkar and Kyu,<sup>13</sup> the crystalline–crystalline interaction parameter  $\chi_{c_1 c_2} \equiv \chi_{\text{cc}}$  can be expressed as a geometric mean of the crystalline–amorphous interactions ( $\chi_{\text{ca}}$  and  $\chi_{\text{ac}}$ ). To account for nonideal crystalline mixing,  $\chi_{\text{cc}}$  is simply taken as  $\chi_{\text{cc}} = c_\omega [(\chi_{\text{ca}})^{1/2} (\chi_{\text{ac}})^{1/2}]$  in which the proportionality constant  $c_\omega$  signifies any departure from ideality (if it is different from unity). The  $c_\omega$  parameter in the geometric mixing rule is analogous to the ' $c$ ' anisotropic interaction defined for the cases of nematic liquid crystal mixtures.<sup>14</sup> Physically,  $c_\omega = \chi_{\text{cc}} / [(\chi_{\text{ca}})^{1/2} (\chi_{\text{ac}})^{1/2}]$  can be interpreted in different cases as follows: (i) For  $c_\omega < 1$ , the interactions between the two constituent crystals are weak, and the formation of separate individual crystals is favored. (ii) For  $c_\omega > 1$ , the formation of cocrystals prevails because of the strong crystalline–crystalline interaction. In the ideal case of  $c_\omega = 1$ , there is no preference for crystal formation of either type.<sup>13</sup>

The crystal order parameter  $\psi_1$  is the linear crystallinity (i.e., in one dimension) of component 1 and thus the product with its volume fraction ( $\psi_1 \phi_1$ ) corresponds to the bulk crystallinity (or crystalline fraction). On the other hand, the product of  $\phi_2$  and  $\psi_1$  signifies the amount of amorphous materials of component 2 interacting with the crystalline phase of component 1. Hence, the term  $\chi_{\text{ca}} \phi_1 \psi_1 \phi_2 \psi_1$  signifies the crystalline–amorphous interaction. The same argument can be made for the second crystalline component,  $\chi_{\text{ac}} \psi_1 \phi_2 \psi_2 \phi_1$ . The cross-interaction term,  $\chi_{\text{cc}} \psi_1 \phi_1 \psi_2 \phi_2$ , can be interpreted as the crystalline–crystalline interaction that occurs when crystals of component 1 ( $\phi_1 \psi_1$ ) attempt to mix with crystals of component 2 ( $\phi_2 \psi_2$ ).

To determine the solid crystal–isotropic liquid phase transition, the free energy is first minimized with respect to the individual crystalline order parameters. Subsequently, a common tangent algorithm can be employed to determine the coexistence lines, as reported elsewhere.<sup>13</sup> Alternatively, the crystalline–amorphous parameter,  $\chi_{\text{ca}}$ , can be determined directly from the experimental melting point depression plot.<sup>15</sup>

## RESULTS AND DISCUSSION

Figure 1 shows the overlay of the DSC and TGA thermograms of genistein along with its chemical structure. The DSC

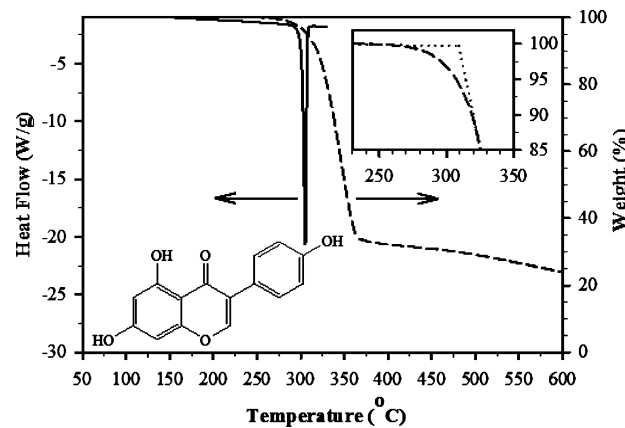


Figure 1. DSC (solid line) and TGA (dashed line) thermograms of neat genistein, yielding  $T_m = 305^\circ\text{C}$  and  $T_d = 309^\circ\text{C}$  (as estimated from the 5 wt % loss), respectively.

endothermic peak at  $305^\circ\text{C}$  is regarded as the crystal melting temperature ( $T_m$ ). According to the TGA measurements, genistein undergoes thermal degradation at an onset temperature of  $275^\circ\text{C}$ , but the intercept of the two slopes occurs at  $309^\circ\text{C}$  (see the inset), which is regarded as the degradation temperature ( $T_d$ ). Consistent with the literature, this temperature ( $T_d$ ) corresponds to the point of 5% weight loss in the TGA thermogram. As is typical for small-molecule crystals, the thermal degradation of genistein takes place at a temperature ( $309^\circ\text{C}$ ) slightly above its crystal melting ( $305^\circ\text{C}$ ).

As can be seen in Figure 2, the DSC endothermic peak for PEO44k appears at  $65^\circ\text{C}$  and is taken as the  $T_m$  of PEO44k

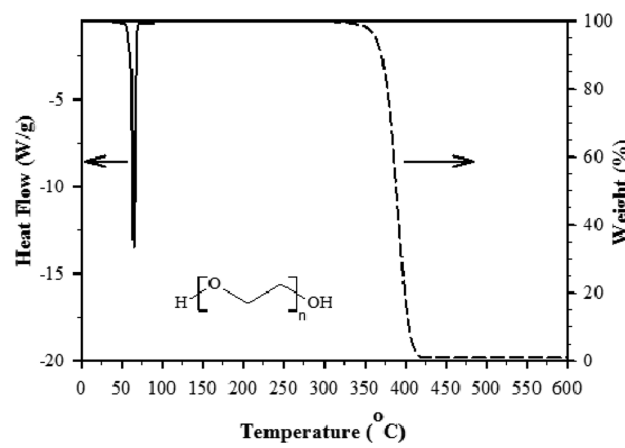
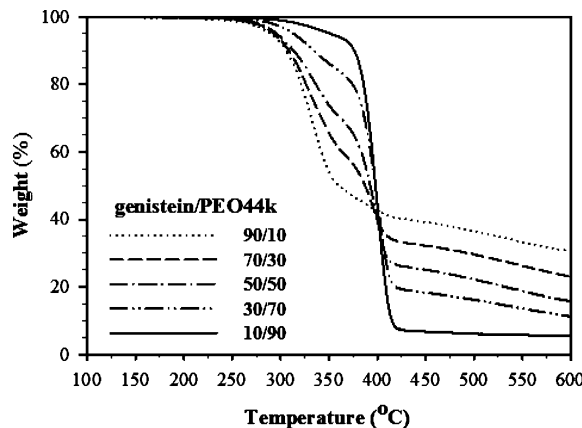


Figure 2. DSC (solid line) and TGA (dashed line) thermograms of neat PEO44k, giving  $T_m = 65^\circ\text{C}$  and  $T_d$  (5 wt % loss) =  $363^\circ\text{C}$ .

crystals. Unlike most small-molecule crystals, PEO44k is remarkably stable, exhibiting thermal degradation at a significantly higher temperature of  $363^\circ\text{C}$ . It is interesting to determine how genistein and PEO44k mutually affect the thermal stability in their blends. Thermogravimetric analysis was performed on various compositions of genistein/PEO44k blends, namely, 10/90, 30/70, 50/50, 70/30, and 90/10. Figure 3 shows TGA weight loss curves of the mixtures, which shift



**Figure 3.** Overlay of TGA thermograms of genistein/PEO44k blends at various blend compositions: dotted line, 90/10; dashed line, 70/30; dash-dotted line, 50/50; dash-dot-dotted line, 30/70; and solid line, 10/90.

systematically with composition between those of the pure components. The intermediate compositions show dual inflections. The first inflection corresponding to the decomposition of the genistein-rich phase shifted subtly to a higher temperature with increasing PEO44k content, whereas the second inflection at higher temperature can be attributed to the thermal decomposition of the PEO44k-rich phase. It can be hypothesized that this enhanced thermal stability of genistein in

its PEO44k blends might be a consequence of some specific interaction such as hydrogen bonding occurring between PEO44k and genistein molecules.

The glass transition of PEO44k was observed at  $-48^{\circ}\text{C}$ . As is typical for a small-molecule system, no  $T_g$  was observable for genistein over the wide temperature range from  $-90$  to  $350^{\circ}\text{C}$  investigated. In the blends, a single glass transition was discernible and shifted systematically toward higher temperature with increasing concentration of genistein. The  $T_g$  value reached  $-7^{\circ}\text{C}$  at 50 wt % genistein, beyond which it was no longer discernible. The dramatic increase of the PEO  $T_g$  value in the blends from  $-48$  to  $-7^{\circ}\text{C}$  implies that the glass transition temperature of genistein, if it exists, would be much higher. The incorporation of rigid genistein molecules into PEO not only hinders the chain motion but also increases miscibility through interspecies hydrogen bonding, thereby raising the  $T_g$  value of their blends. However, it should be borne in mind that the existence of a single glass transition in a limited composition range is not sufficient proof for determining miscibility between the noncrystalline genistein and PEO44k pair.

Figure 4a shows DSC thermograms of a series of genistein/PEO44k blends arranged vertically as a function of composition. The endothermic peaks of pure genistein and PEO44k are omitted here for clarity and can be found in Figures 1 and 2, respectively. The results for extreme compositions (PEO44k-rich and genistein-rich samples), which are not well resolved, are magnified and shown in the

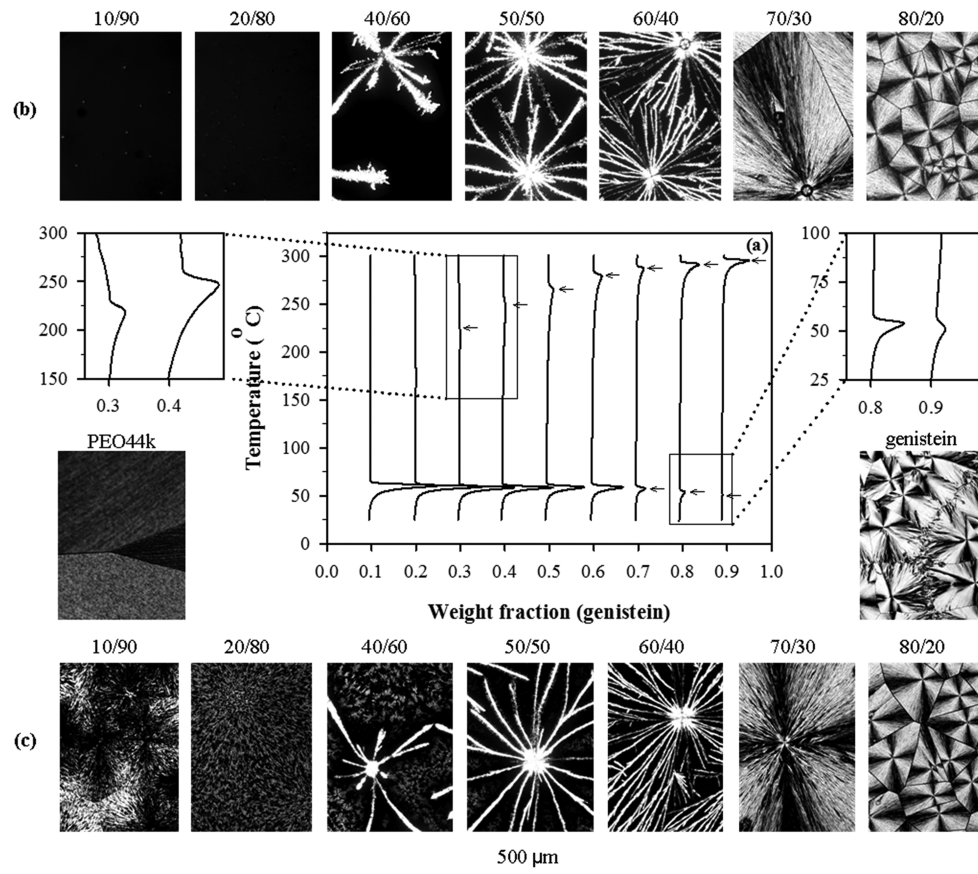


**Figure 4.** (a) DSC thermograms of genistein/PEO44k blends at various blend compositions. The enlarged phase diagrams show melting points of genistein at weight fractions of 0.3 and 0.4 and melting points of PEO44k at weight fractions of 0.8 and 0.9. (b,c) Phase morphologies of genistein/PEO44k blends observed under a crossed polarizer at two different temperatures: (b) 200 and (c)  $25^{\circ}\text{C}$ .

enlarged figures. Except for samples of PEO44k-rich compositions, all samples exhibited dual endothermic peaks in the temperature ranges of 225–300 °C and 55–65 °C, corresponding to the  $T_m$  values of genistein and PEO44k crystals, respectively. The melting endothermic peaks of genistein crystals in the mixtures decreased as the PEO44k concentration increased. However, the melting peaks of PEO44k showed little or no movement up to 70 wt % genistein, but a slight decline at higher concentrations of 80 and 90 wt %.

To examine phase behavior, the morphology of genistein/PEO44k blends was examined at various temperatures and compositions using a polarizing optical microscopy. The POM micrographs are shown together with the DSC thermograms in Figure 4. At room temperature, PEO44k spherulites thus developed were so large that only the grain boundary due to the impingement effect could be discerned at 50× magnification. However, typical spherulites on the order of ~500 μm can be seen in pure genistein with distinct grain boundaries among these impinged spherulites.

A series of POM images representing the emerged phase morphologies of the genistein/PEO44k blends at 200 °C are displayed in the upper row of Figure 4. The completely dark appearances under the cross-polarizers, as well as the lack of any identifiable domains under parallel polarization, suggest that the PEO44k-rich compositions (i.e., 10 and 20 wt % genistein) belong to a single-phase region. However, the existence of the crystalline + isotropic region can be identified at higher genistein loadings. For instance, in the 40/60 genistein/PEO44k composition, a seaweed or needlelike lamellar structure develops, fanning out from a common core in the continuum of dark isotropic background, suggestive of the isotropic liquid + crystal coexistence region. The population of these radiating needlelike lamellae increased with increasing genistein content (up to 60 wt %). Eventually, these lamellae aggregated to a more complex structure called a "sheaflike" texture at 70 wt % and then fully developed to spherulites with further increase of genistein to 80 wt %.

Crystalline phase morphologies of the genistein/PEO44k blends at room temperature are illustrated in the bottom row of Figure 4. Two distinct crystalline structures, needlelike lamellae radiating from the common core and open (loosely organized) spherulites, were clearly observed at intermediate compositions (40–60 wt % genistein), indicating the crystalline + crystalline coexistence phase. However, the existence of two crystalline morphologies was not well resolved at the extreme compositions because of domination by the spherulitic structures of one or the other constituent.

Based on the morphological observations and the DSC phase transitions, a theoretical phase diagram of genistein/PEO44k blends was calculated self-consistently using the experimental parameters ( $\Delta H_1 = 8,400 \text{ J/mol}$ ,  $\Delta H_2 = 9,020 \text{ J/mol}$ ,  $T_{m,1}^o = 305 \text{ }^\circ\text{C}$ ,  $T_{m,2}^o = 65 \text{ }^\circ\text{C}$ ) and material parameters ( $r_1 = 1$ ,  $r_2 = 24$ ,  $T_{crit} = -30 \text{ }^\circ\text{C}$ ,  $A = 0$ ,  $\chi_{ac} = 0.65$ ,  $\chi_{ca} = 1.50$ , and  $c_\omega = 0.1$ ). Note that the materials parameters  $r_1$  and  $r_2$  were estimated from the molecular weight of each constituents, whereas  $\chi_{ac}$  and  $\chi_{ca}$  were estimated from the heats of fusion of the constituent crystals.  $T_{crit}$ ,  $A$ , and  $c_\omega$  were used as adjustable parameters. As shown in Figure 5, the liquidus and solidus lines thus obtained from the self-consistent solution reveal a eutectic-type phase diagram with the eutectic point at ~7 wt % genistein and at 62 °C. The calculated liquidus lines are in good accord with the experimental melting transition points. However, the calculated

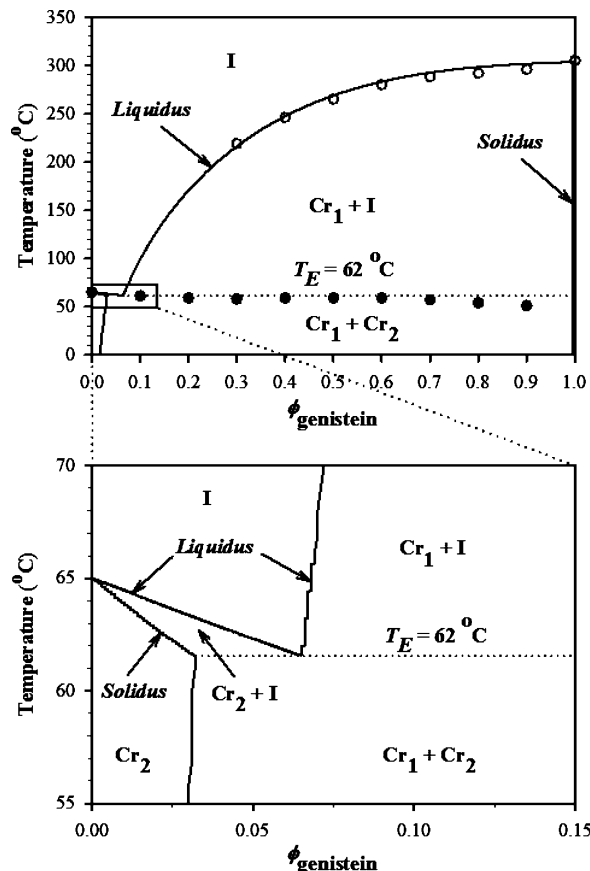


**Figure 5.** Theoretical phase diagram of genistein/PEO44k blends in comparison with the melting temperatures obtained by DSC. The eutectic phase diagram shows various coexistence regions: I, isotropic phase;  $\text{Cr}_1 + \text{I}$ , crystal 1 + isotropic region;  $\text{Cr}_2 + \text{I}$ , crystal 2 + isotropic region;  $\text{Cr}_1$ , pure crystalline 1 (genistein); and  $\text{Cr}_2$ , pure crystalline 2 (PEO44k). The solid line denotes the theoretical curve calculated based on the combined theories of Flory–Huggins and extended phase field. The symbols represent (○)  $T_m(\text{genistein})$  and (●)  $T_m(\text{PEO44k})$ . The enlarged phase diagram reveals a narrow  $\text{Cr}_2 + \text{I}$  coexistence region.

solidus lines virtually coincide with the neat-component axes, which are very difficult to determine experimentally. The calculated phase diagram exhibits a variety of single-phase and coexistence regions, including isotropic (I), crystal + isotropic liquid ( $\text{Cr}_1 + \text{I}$  and  $\text{Cr}_2 + \text{I}$ ) coexistence regions, and single-crystalline phases ( $\text{Cr}_1$  and  $\text{Cr}_2$ ). Although the idea of taking a eutectic melting approach for solubilizing genistein in PEO44k is interesting in its own right, the observed solid crystalline + crystalline ( $\text{Cr}_1 + \text{Cr}_2$ ) region extending over the entire composition range at the body temperature (37 °C) needs significant improvement. The lack of solubility of genistein in PEO44k would prevent any application of genistein/PEO44k in oral administration or injectable formulation.

To overcome the aforementioned obstacle, it is necessary to lower the eutectic temperature below body temperature. A simple but effective solution is to incorporate a lower-molecular-mass analogue, such as poly(ethylene glycol), into genistein. The hydroxyl end groups of PEG also have an added advantage in solubilizing genistein. DSC analysis was employed in a similar fashion. The crystal melting point of PEG with a molecular weight of 6700 g/mol (designated as PEG7k) was reduced to 57 °C, and it dropped to 2 °C with a further

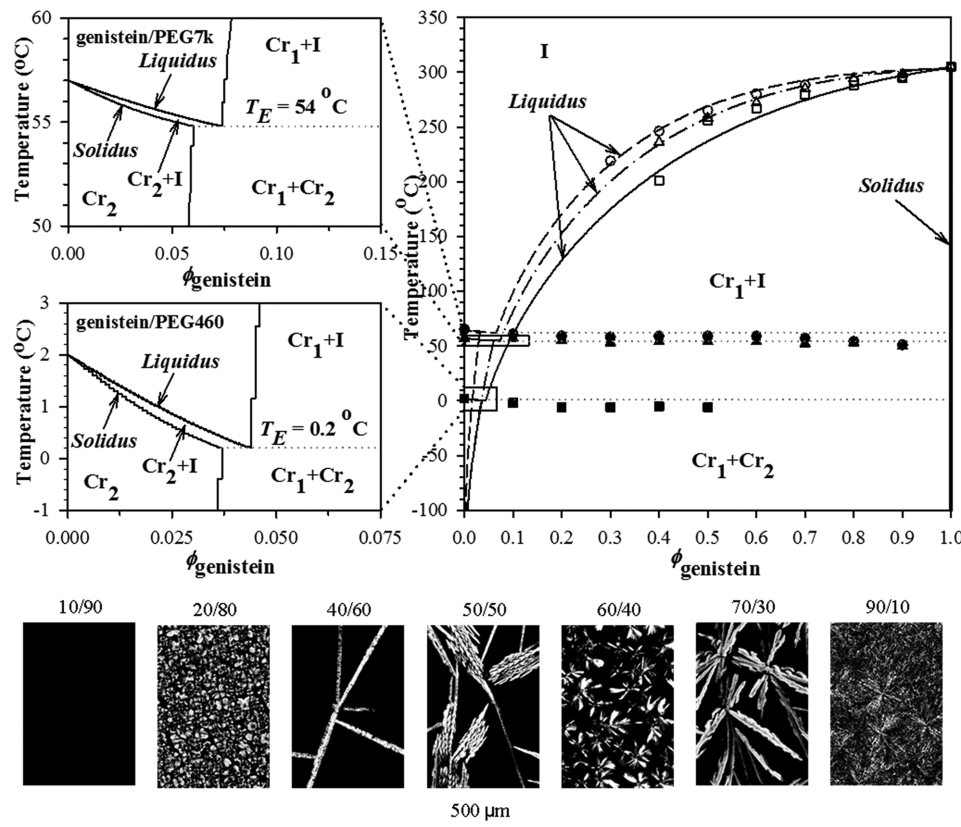


**Figure 6.** Theoretical and experimental phase diagrams of genistein/PEG7k (dash-dotted line) and genistein/PEG460 (solid line) blends in comparison with those of genistein/PEO44k (dashed line) blends. The eutectic phase diagram shows various coexistence regions: I, isotropic phase; Cr<sub>1</sub> + I, crystal 1 + isotropic region; Cr<sub>2</sub> + I, crystal 2 + isotropic region; Cr<sub>1</sub>, pure crystalline 1 (genistein); and Cr<sub>2</sub>, pure crystalline 2 (PEO44k, PEG7k, or PEG460). The open symbols [○, △, □, T<sub>m</sub>(genistein)] and the solid symbols [●, T<sub>m</sub>(PEO44k); ▲, T<sub>m</sub>(PEG7k); ■, T<sub>m</sub>(PEG460)] represent melting points observed in these three binary eutectic systems. The enlarged phase diagram of genistein/PEG7k and genistein/PEG460 shows the Cr<sub>2</sub> + I coexistence region. Photomicrographs show the phase morphologies of genistein/PEG460 blends observed under a crossed polarizer at 25 °C.

decrease of the molecular weight to 460 g/mol (hereafter designated as PEG460). The trend of melting point depression was observed in both genistein/PEG systems, exhibiting eutectic behavior. The eutectic point of genistein/PEG7k blends was found at 54 °C. The eutectic temperature declined to 0.2 °C when the molecular weight of PEG was lowered to 460 g/mol. For genistein/PEG7k, the liquidus and solidus lines were obtained by self-consistent solution. We used the experimental parameters ( $\Delta H_1 = 8,400 \text{ J/mol}$ ,  $\Delta H_2 = 7,500 \text{ J/mol}$ ,  $T_{m,1}^{\circ} = 305 \text{ }^{\circ}\text{C}$ ,  $T_{m,2}^{\circ} = 57 \text{ }^{\circ}\text{C}$ ) and material parameters ( $r_1 = 1$ ,  $r_2 = 15$ ,  $T_{\text{crit}} = -70 \text{ }^{\circ}\text{C}$ ,  $A = 0$ ,  $\chi_{ac} = 0.51$ ,  $\chi_{ca} = 2.88$ , and  $c_{\omega} = 0.12$ ) in the calculation. Because PEG7k shows limited improvement in depressing the eutectic temperature, we focused only on the PEG460 system. The material and experimental parameters used in the calculation of the eutectic phase diagram of genistein/PEG460 were  $r_1 = 1$ ,  $r_2 = 5$ ,  $\Delta H_1 = 8400 \text{ J/mol}$ ,  $\Delta H_2 = 3300 \text{ J/mol}$ ,  $T_{m,1}^{\circ} = 305 \text{ }^{\circ}\text{C}$ ,  $T_{m,2}^{\circ} = 2 \text{ }^{\circ}\text{C}$ ,  $T_{\text{crit}} = -150 \text{ }^{\circ}\text{C}$ ,  $A = -0.3$ ,  $\chi_{ac} = 0.12$ ,  $\chi_{ca} = 2.60$ , and  $c_{\omega} = 0.18$ . The liquidus lines, obtained self-consistently, captured the trends of depressed melting transition points meeting at the eutectic point.

Figure 6 shows the eutectic phase diagram of genistein/PEG mixtures (represented by the dot-dashed lines for PEG7k and the solid lines for PEG460) in comparison with that of the genistein/PEO44k blend (dashed lines). The enlarged figure near the eutectic point reveals a narrow Cr<sub>2</sub> + I coexistence region for the PEG7k system, but the eutectic point (54 °C) is

still too high to solubilize genistein at body temperature. This is a reaffirmation of our strategy to focus only on the genistein/PEG460 mixture. With a polymeric constituent of lower molecular weight (PEG460), the crystal-crystal coexistence curve and crystal-liquid coexistence region are thrust farther downward with the eutectic point at 0.2 °C and ~4 wt % genistein. As evidenced in the single-crystal region of PEG (Cr<sub>2</sub>) becoming wider relative to that of PEO44k at the same temperature, better solubility of genistein occurs upon lowering the molecular weight of PEG.

The phase morphologies of genistein/PEG460 blends at room temperature, illustrated at the bottom of Figure 6, were also congruent with our calculations. No evidence of crystals was observed under the cross-polarizer configuration, especially for the mixture containing less than 10 wt % genistein. At higher genistein concentrations, the coexistence crystal + isotropic region was confirmed, with the needlelike (or sheaflike) genistein crystals in the continuum of isotropic genistein/PEG460 liquid.

The observed depression of the eutectic point in the phase diagram below room temperature is significant because this means that genistein can be solubilized in PEG460. Theoretically, the depressed eutectic point has been hitherto explained simply by the lowering of the molecular weight of the constituent POE, that is, from PEO44k to PEG460. Given the chemical structures of genistein and PEO or PEG, interspecies hydrogen bonding can occur between the hydroxyl of genistein

and not only the oxygen ether of PEO or PEG, but also the terminal hydroxyl groups of PEG460. Compared with PEO44k, PEG460 contains higher numbers of terminal hydroxyl groups. Therefore, PEG460 has greater opportunity to undergo interspecies hydrogen bonding with hydroxyl groups of genistein molecules.

Figure 7 shows the FTIR spectra of neat genistein, neat PEO44k, and their mixtures in the 3600–1000 cm<sup>-1</sup> range.

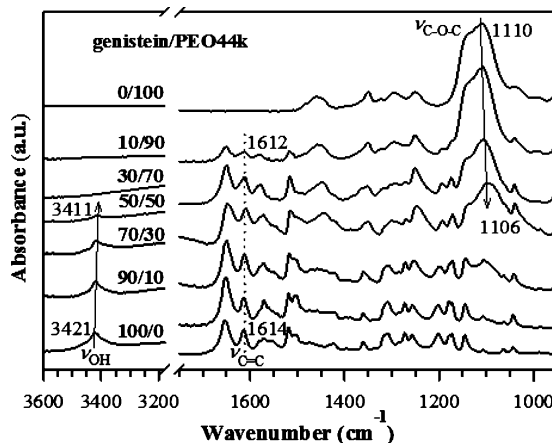


**Figure 7.** FTIR spectra of neat genistein, neat PEO44k, and genistein/PEO44k blends at five different compositions (10/90, 30/70, 50/50, 70/30, 90/10), scanned at 100 °C.

These FTIR experiments were carried out at 100 °C for both genistein/PEO44k and genistein/PEG460 mixtures to alleviate moisture absorption, if any. The hydroxyl groups of genistein can undergo both intra- and intermolecular self-association as well as interspecies interactions with its polymer counterpart in blends. That is, the hydroxyl groups of genistein can form hydrogen bonds with the proton-accepting group, that is, the ether oxygen (or C—O—C) of PEO44k. Genistein exhibits a broad peak centered at 3421 cm<sup>-1</sup>, attributable to the hydroxyl-stretching ( $\nu_{\text{O}-\text{H}}$ ), whereas PEO44k does not have such a characteristic band in this region. The  $\nu_{\text{O}-\text{H}}$  peak of genistein systematically shifts to a lower wavenumber of 3411 cm<sup>-1</sup> with the addition of PEO44k up to 50 wt %, beyond which the peak is no longer detectable. This spectral change is rather complex and is seemingly governed by competition between the self-associated hydrogen bonds in genistein molecules and interspecies hydrogen bonds between genistein and PEO44k. In this scheme, the cross-hydrogen bonding of PEO44k with genistein would contribute to a lower wavenumber of the  $\nu_{\text{O}-\text{H}}$  peak, whereas the self-associated hydroxyl groups of genistein would contribute to the spectral peak moving to a higher wavenumber due to greater mobility. Depending on the relative contributions of each effect, the spectral shift can go in either direction. The observed shift of the  $\nu_{\text{O}-\text{H}}$  peak to a lower wavenumber implies that interspecies hydrogen bonding is dominant. The possible interspecies hydrogen bonding can be further examined based on the asymmetric C—O—C stretching ( $\nu_{\text{C}-\text{O}-\text{C}}$ ) band of PEO appearing at 1110 cm<sup>-1</sup>. This band moves to a slightly lower wavenumber by about 4 cm<sup>-1</sup> in the 50 wt % blend, which is within the resolution of the IR experiments (4 cm<sup>-1</sup>). However, this 4 cm<sup>-1</sup> shift is slightly larger than the characteristic band that is not involved in any specific interactions, such as the aromatic C=C stretching band of genistein, and is virtually stationary (i.e., less than 2

cm<sup>-1</sup> fluctuations). Both the limited movement of the  $\nu_{\text{O}-\text{H}}$  peak and the minor movement of the  $\nu_{\text{C}-\text{O}-\text{C}}$  peak suggest the possibility of interspecies hydrogen bonding, albeit weak, occurring between phenolic hydroxyl groups of genistein and the ether oxygen of PEO44k.

Unlike the genistein/PEO44k system, the presence of the terminal hydroxyl groups in PEG460 provides additional sites for interspecies hydrogen bonding with genistein. Because this hydroxyl group is located only at the chain ends, the intramolecular hydrogen bonding between hydroxyl and oxygen ether of PEG460 would be negligibly small relative to the self-associating intermolecular hydrogen bonds among PEG molecules. As shown in Figure 8, the FTIR spectrum of pure

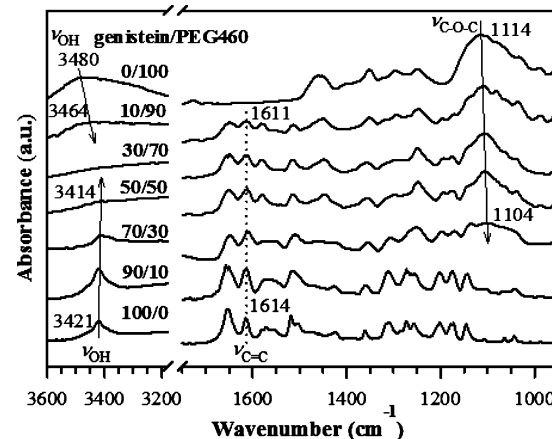


**Figure 8.** FTIR spectra of neat genistein, neat PEG460, and genistein/PEG460 blends at five different compositions (10/90, 30/70, 50/50, 70/30, 90/10), scanned at 100 °C.

PEG460 reveals a broad peak at 3480 cm<sup>-1</sup>, attributable to the terminal hydroxyl group. It should be emphasized that this  $\nu_{\text{O}-\text{H}}$  band moves to a lower wavenumber (3464 cm<sup>-1</sup>) upon the incorporation of 10 wt % genistein before it gradually becomes less distinct at 30 wt % genistein. The phenol hydroxyl stretching vibration band of neat genistein (3421 cm<sup>-1</sup>) also shifts to a lower wavenumber of 3414 cm<sup>-1</sup> with increasing PEG460 concentration up to 50 wt %, whereas the  $\nu_{\text{C}-\text{O}-\text{C}}$  band of PEG460 shows a shift of about 10 cm<sup>-1</sup> with increasing genistein content up to 70 wt %. The movement of this band implies hydrogen bonding of the hydroxyl groups of genistein with the hydroxyl end group of PEG460 molecules, and to a lesser extent to the ether oxygen of PEG460. The occurrence of interspecies hydrogen bonding probably contributes to better solubility of genistein in PEG, especially at low genistein concentrations (e.g., ~7 wt % at room temperature).

## CONCLUSIONS

We have demonstrated experimentally and theoretically the eutectic crystal melting approach as a means of solubilizing genistein in poly(ethylene glycol) solution. The self-consistently calculated liquidus curves were found to agree well with the depressed melting points obtained from the DSC experiments, whereas the solidus lines coincide with the neat-genistein axis. Of particular importance is the lowering of the eutectic temperature of genistein/PEO44k blend from 62 to 0.2 °C upon switching to the genistein/PEG460 system. The occurrence of interspecies hydrogen bonding between genistein molecules and both PEO44k and PEG460 chains, albeit weak,

was noticed in the examination by FTIR spectroscopy. The improved solubility of genistein in PEG460 can be attributed not only to the lower molecular weight of PEG460 utilized, but also to the terminal hydroxyl groups forming interspecies hydrogen bonds with hydroxyl groups of genistein. At ambient temperature, approximately 7 wt % genistein was found to be soluble in PEG460. It can be anticipated that the present findings provide new development for genistein-containing drugs for oral administration by overcoming one of the impediments in pharmaceutical crystals, that is, finding an appropriate solvent.

## ■ AUTHOR INFORMATION

### Corresponding Author

\* E-mail: tkyu@uakron.edu. Tel.: (330) 972-6672. Fax: (330) 972-3406.

### Notes

The authors declare no competing financial interest.

## ■ ACKNOWLEDGMENTS

This work was supported by the Ohio Soybean Council (OSC). S.B. is indebted to the Royal Thai Government (RTG) for support.

## ■ REFERENCES

- (1) Hong, H.; Landauer, M. R.; Foriska, M. A.; Ledney, G. D. *J. Basic Microbiol.* **2006**, *46* (4), 329–335.
- (2) Verdrengh, M.; Collins, L. V.; Bergin, P.; Tarkowski, A. *Microbes Infect.* **2004**, *6*, 86–92.
- (3) Wei, H.; Cai, Q.; Rahn, R. O. *Carcinogenesis* **1996**, *17*, 73–77.
- (4) Thornfeldt, C. *Dermatol. Surg.* **2005**, *31* (7), 874–880.
- (5) Xi, J.; Guo, R. *J. Solution Chem.* **2009**, *38*, 1588–1600.
- (6) Motlekar, N.; Khan, M. A.; Youan, B-B. C. *J. Appl. Polym. Sci.* **2006**, *101*, 2070–2078.
- (7) Liu, R. *Water-Insoluble Drug Formulation*; CRC Press: Boca Raton, FL, 2008.
- (8) Hilderbrand, J. H.; Scott, R. L. *The Solubility of Nonelectrolytes*; Reinhold Publishing Corporation: New York, 1950.
- (9) Scott, P. W.; Williams, A. C.; Barry, B. W. *J. Controlled Release* **1998**, *50*, 298–307.
- (10) Fuertges, F.; Abuchowski, A. *J. Controlled Release* **1990**, *11*, 139–148.
- (11) Flory, P. J. *J. Chem. Phys.* **1947**, *15*, 684.
- (12) Kobayashi, R. *Physica D* **1993**, *63*, 410–423.
- (13) Matkar, R. A.; Kyu, T. *J. Phys. Chem. B* **2006**, *110*, 16059–16065.
- (14) Chiu, H. W.; Kyu, T. *J. Chem. Phys.* **1998**, *108* (8), 3249–3255.
- (15) Rathi, P.; Huang, T.-M.; Dayal, P.; Kyu, T. *J. Phys. Chem. B* **2008**, *112*, 6460–6466.